Clays and Clay Minerals, Vol. 58, No. 3, 340–350, 2010.

NEW TEMPLATE EFFECT IN HYDROTALCITE SYNTHESIS. NODULAR *VS.* LAYERED MORPHOLOGIES

ALICIA E. SOMMER[1], GEOLAR FETTER[1,*], PEDRO BOSCH[2], AND VICTOR H. LARA[3]

[1] Universidad Autónoma de Puebla, Facultad de Ciencias Químicas, Blvd. 14 Sur y Av. San Claudio, 72570 Puebla, PUE, Mexico

[2] Universidad Nacional Autónoma de Mexico, Instituto de Investigaciones en Materiales, Ciudad Universitaria, 04510 Mexico, D.F., Mexico

[3] Universidad Autónoma Metropolitana – Iztapalapa, Departamento de Química, Av. Michoacán esq. Purísima, 09340 México, D.F., Mexico

Abstract—The morphology of hydrotalcites determines their use in catalysis, biomedicine, or adsorption as they may work as anion exchangers or as drug deliverers. In catalysis, reagents need access to as much surface area as possible; in biomedicine, drugs have to be encapsulated. However, the parameters and the mechanisms which direct the synthesis towards a certain morphology are not well understood. Precipitating agents or crystallization conditions are expected to play a crucial role. In the present study, hydrotalcites were synthesized in the presence of two precipitating agents (NaOH or NH_4OH) under three different crystallization conditions (conventional, microwave, or ultrasound irradiation) which determined the morphology of the final product, layered or vesicular. The features are explained through the template effect of the liberated gases on the co-precipitation and crystallization processes and consequently on the final structure/morphology of the synthesized solids. Indeed, the nodular particles crystallize using the effluent gases as templates. Fractal dimension and particle-size distributions, determined by small-angle X-ray scattering (SAXS) and gas adsorption are compared and correlated to the presence of ammonium. Although the materials obtained are heterogeneous, it is possible to propose a microscopic geode model.

Key Words—Ammonium Hydroxide, Globular, Hydrotalcite, Microwave Irradiation, Nanoporosity, Nodule, Spherical Materials, Ultrasound Irradiation, Vesicle.

INTRODUCTION

Layered double hydroxides (LDH), hydrotalcite-like compounds, or hydrotalcites are porous materials. They are used in catalysis, adsorption, and ion exchange among other things (Li and Duan, 2006; Allada *et al*., 2006; Sels *et al*., 2001; Tichit and Vaccari, 1998). The layered double hydroxides are anionic clays as they have positively charged layers due to a partial substitution of a divalent metal, such as Mg^{2+}, by a trivalent one, such as Al^{3+}. The charge is compensated by anions and water molecules intercalated between the layers. The LDH materials are represented by the general formula $[M^{2+}_{1-x}M^{3+}_{x}(OH)_2](A^{m-})_{x/m}.nH_2O$ where M^{2+} and M^{3+} are the di- and trivalent metals, respectively, and A^{m-} is a compensating anion (Cavani *et al*., 1991; Rives and Ulibarri, 1999). Although various LDHs can be obtained by modifying the composition and the synthesis process, the most common LDH is $Mg_6Al_2(OH)_{16}CO_3.4H_2O$ which represents the natural hydrotalcite structure. The usual synthesis procedure is co-precipitation of the cationic metals in a basic medium (NaOH), followed by a conventional hydrothermal treatment (Evans and Slade, 2006; He *et al*., 2006).

Although some authors report the use of ammonium hydroxide in the synthesis of hydrotalcites (Lopez *et al*., 1996; Olanrewaju *et al*., 2000; Paredes *et al*., 2006; Lei *et al*., 2006), special attention has not been focused on the effect of ammonium on the morphology of these solids. Indeed, the ammonium ions, present in the synthesis gel, decompose to ammonia gas during the hydrothermal treatment (crystallization step). When this gas flows out as bubbles through the slurry some structural modifications should be expected. To date, the process has not been described or studied and may be used to control the final particle morphology by modifying the rate at which the templating bubbles are formed. Indeed, the size and the frequency of those templating agents should be a function of the crystallization mode.

In the present study, the synthesis of hydrotalcite-like compounds with ammonium hydroxide as a precipitant is described, employing microwave or ultrasound irradiation in the hydrothermal step. On the one hand, the treatments during the hydrothermal step determine the crystallinity, texture, and morphology of the resulting compounds, and on the other, the use of ammonium hydroxide is relevant if compared to the conventional NaOH precipitating agent which does not liberate gases.

* E-mail address of corresponding author:
geolarfetter@yahoo.com.mx
DOI: 10.1346/CCMN.2010.0580305

https://doi.org/10.1346/CCMN.2010.0580305 Published online by Cambridge University Press

Non-conventional parameters such as fractal dimension or particle-size distributions are correlated with the synthesis conditions and the presence of ammonium.

EXPERIMENTAL

Hydrotalcite synthesis

Mg/Al-hydrotalcite samples were synthesized from a $Mg(NO_3)_2.6H_2O$ and $Al(NO_3)_3.9H_2O$ (both from Aldrich) 3.3 M water solution. A second aqueous solution, 2 M, was prepared using NH_4OH (Baker). The precipitation was carried out at a constant pH of 10 (±0.5) by adjusting the flow of each solution. The solution amounts corresponded to a molar Mg/Al ratio of 3. After precipitation, the resulting gels were heat treated in one of three different ways. (1) They were heated in a microwave autoclave (MIC-I, Sistemas y Equipos de Vidrio S.A. de C.V.) for 10 min at 80ºC and 1 atm, operating at 2.45 GHz and a power of 200 W (sample referred to as NH_4MW). Note that temperature was controlled by means of an infrared radiation sensor, and a stirring mechanism adapted to the autoclave ensured that temperature was the same throughout. A constant pressure was maintained by a control-valve system. (2) They were sonicated in an ultrasound reservoir (open vessel of 400 mL capacity) (Cole-Palmer B200) operating at 2.4 kW and 25 kHz; the temperature was fixed at 80ºC (sample NH_4US). (3) They were heated in a conventional way, *i.e.* the reactor was an open vessel heated on a magnetic stirrer plate in which the mixture was stirred continuously for 24 h at room temperature (25ºC) (sample NH_4CON). After the hydrothermal treatments the solids were recovered by decantation and washed several times with distilled water until the residual solution reached a pH value of 8.7 (±0.2). The solids were then dried in an oven at 70ºC overnight. A fourth sample was synthesized in the same way as for the sample NH_4MW but employing NaOH solution instead of NH_4OH solution in the precipitation step (sample NaMW).

Characterization

X-ray diffraction. A Bruker-AXS D8-advance diffractometer coupled to a copper anode X-ray tube was used to identify the compounds present in the powdered samples. A diffracted-beam monochromator selected the Kα radiation. The thermodiffraction patterns were recorded in a Siemens D5000 diffractometer with a copper anode tube and a heating rate of 10ºC/min.

Fourier transform infrared spectroscopy. The FTIR spectra in the region 4000−400 cm^{-1} were obtained using a Nicolet Model Magna-550 IR Spectrometer. The pellets were prepared by dispersing 2 wt.% of sample in KBr.

Nitrogen adsorption. The BET surface areas were determined from the nitrogen adsorption-desorption curves by the conventional multipoint technique with a Micromeritics ASAP 2020. The pore-size distribution curves were obtained using the BJH (Barrer-Joyner-Halenda) method applied to the desorption branch. The samples were pretreated at 200ºC for 10 h at high vacuum. At this temperature the hydrotalcite was stable as shown by the X-ray thermodiffraction patterns presented in the results section.

Thermal analysis. Thermogravimetric and differential thermal analysis (TGA-DTA) were carried out with 50 mg of sample heated from room temperature to 600ºC at the rate of 10ºC/min, in CO_2 atmosphere, using a TA Instruments device.

Small angle X-ray scattering. A Kratky camera was used with Ni-filtered CuKα radiation to measure the small-angle X-ray scattering (SAXS) curves. The distance between the sample and the linear proportional counter was 25 cm. The sample was introduced to the beam via a capillary tube. Intensity $I(h)$ was measured for 9 min in order to obtain good-quality statistics. The SAXS data were processed using the ITP program (Glatter, 1988; Glatter and Gruber, 1993) where the angular parameter (h) was defined as $h = 2\pi\sin\theta/\lambda$, where θ and λ are the X-ray scattering angle and the wavelength, respectively. The shape of the scattering objects was estimated from the Kratky plot, *i.e.* $h^2.I(h)$ *vs.* h. The shape was determined depending on the Kratky curve profile; if the curve presented a peak, the particles are globular (bubbles). If a shape can be assumed, the size-distribution function may be calculated. Finally, estimating the fractal dimension of the scattering objects (Harrison, 1995; Martin and Hurd, 1987), from the slope of the curve Log $I(h)$ *vs.* Log(h), is often useful. For this study the background obtained with the Porod plot (Kim, 2004) was removed from the experimental intensity. The h interval was $0.07<h<0.18$ $Å^{-1}$. Note that, by the Babinet principle (Méheust *et al*., 2007), the SAXS may be due either to dense particles in a low-density environment or to pores (or low-density inclusions) in a continuous high electron density medium. In the present study, the word 'heterogeneity' was used to refer to the scattering objects which may be pores or particles.

Scanning electron microscopy (SEM). A LEICA Stereoscan 440 scanning electron microscope was used to study samples which had previously been covered with gold to avoid charging problems.

Tranmission electron microscopy (TEM). A JEOL model JEM-1200eV transmission electron microscope was used at 120 kV. The samples were mounted on a holey carbon film sample holder. Only sample NH_4US was studied with this technique.

Atomic Force Microscopy (AFM). AFM images were obtained from samples NH_4CON and NH_4US. In each

https://doi.org/10.1346/CCMN.2010.0580305 Published online by Cambridge University Press

case, a three-dimensional image was obtained. The images were compared to find similarities and differences between the morphologies. A JEOL JSPM4210 Scanning Probe Microscope was used to obtain images and maps in 3-D using a *WinSPM* program System.

RESULTS

Structure

The ammonium effect on the structure of hydrotalcites was studied by comparing the different hydrothermal treatments such as microwave or ultrasound irradiations. The XRD patterns of all the samples (Figure 1) correspond to hydrotalcite (JCPDS 22-0700); no other crystalline compounds were identified.

For hydrothermal treatments carried out by microwave irradiation (sample NH_4MW) or conventional means (sample NH_4CON), the 00l peak was intense and sharp, showing that both hydrotalcites were well crystallized. The interlayer distance, determined from the 003 peak position, was 8.4 Å. Carbonate-intercalated hydrotalcite is known to have an interlayer distance of 7.7 Å whereas the spacing with nitrate-intercalation is 8.8 Å (Cavani *et al*., 1991). The observed distance is between these, suggesting that it may be an average of the nitrate- and carbonate-intercalated fractions in the sample.

If the sample was treated by sonication (sample NH_4US), the diffraction pattern was similar to those of the previous samples, except the peak intensities were much less. The material, therefore, apparently consists of smaller, well stacked particles. The interlayer distance value for this sample was also 8.4 Å. Note that in both the microwave and the ultrasound irradiated samples, the irradiation time was 10 min. Ultrasound irradiation apparently has to be applied for a longer period to provide enough energy to obtain a well crystallized hydrotalcite.

The reference sample (NaMW) prepared with NaOH gave a similar XRD pattern to those of the previous samples. The interlayer distance determined was 7.6 Å, consistent with it being a carbonate-intercalated sample. Peaks of the 110 and 130 reflections, in the 58−63º2θ interval, were resolved and showed that the long-range order in the layers is better in the reference sample than in the ammonium-containing samples, *i.e*. in the *a* and *b* directions.

Ammonium, nitrate, and carbonate species

The IR spectra of ammonium hydroxide and ammonium chloride were also analyzed for comparison purposes (Figure 2). The corresponding spectra contain bands attributed to functional N-H groups (Pretsch *et al*., 2000) at 795, 1405, and 1753 cm^{-1}. In all hydrotalcite samples with NH_4OH, the 828 cm^{-1} band could be the shifted 795 cm^{-1} band due to the interaction with the hydrotalcite or it may even be attributed to the nitrate ν_2 vibrational mode (Hernández-Moreno *et al*., 1985). The N-H group at 1405 cm^{-1} is overlapped by the intense interlayered 1393 cm^{-1} band of the nitrates (Lopez *et al*., 1997; Rivera *et al*., 2007). The band at 1753 cm^{-1} is at 1762 cm^{-1} in the hydrotalcite. The ammonium ion thus appears to be incorporated into the hydrotalcite structure without great perturbation.

The characteristic band for carbonate at 1365 cm^{-1} is masked in the NH_4OH-containing compounds and hydro-

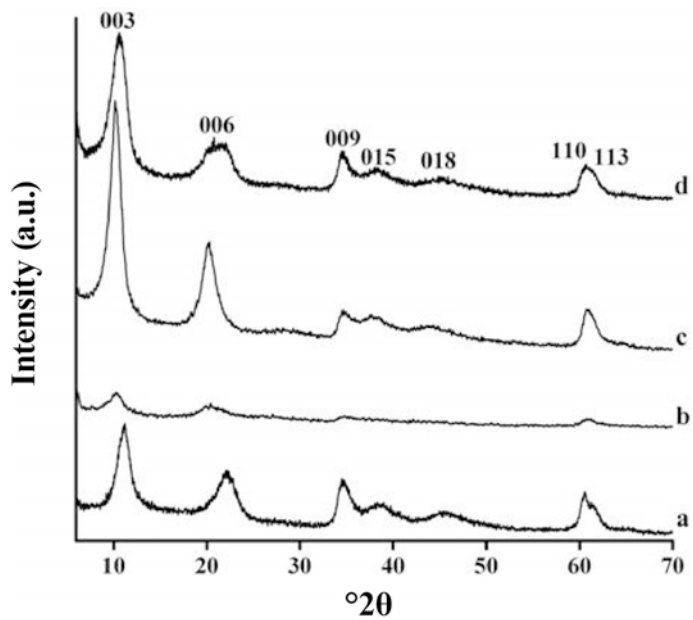


Figure 1. XRD patterns of samples: (a) NaMW; (b) NH_4US; (c) NH_4MW; and (d) NH_4CON.

https://doi.org/10.1346/CCMN.2010.0580305 Published online by Cambridge University Press

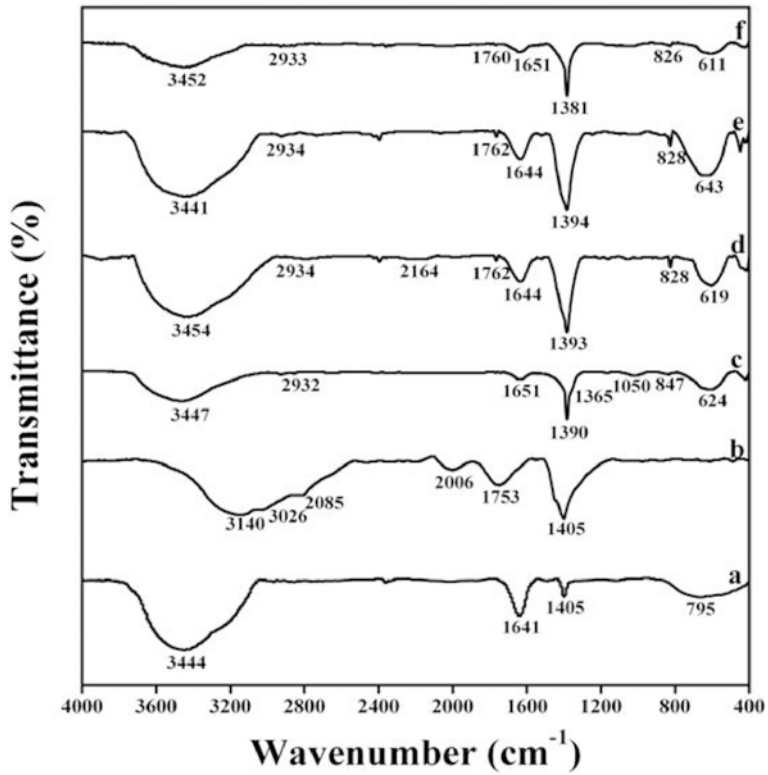


Figure 2. IR spectra of: (a) ammonium hydroxide; (b) ammonium chloride and the hydrotalcite samples; (c) NaMW; (d) NH_4US; (e) NH_4MW; and (f) NH_4CON.

talcites, as expected, because of the N-H bending vibrations. In the reference sample, NaMW, however, a small shoulder at this frequency is noted and the carbonate ν_1 mode is also visible at ~1037 cm^{-1}, revealing the disordered nature of the interlayer (Cavani *et al*., 1991). The broad band at 3441–3452 cm^{-1} and the band at 1648 cm^{-1} are due to the OH-stretching and -bending bands of adsorbed and structural water (Cavani *et al*., 1991).

Morphology

Sample NH_4CON consisted of large, irregular, compact chunks (90 μm) with a smooth, neat surface composed of smaller nodular particles (4 μm), as shown by SEM (Figure 3). The morphology resembles a bowl full of marbles (Figure 3b–d). The particles appear to be stuck together, as if coalescing. Apparently, the small particles are only formed inside the 90 μm chunk. An AFM image reveals that the globular particles are regular, homogeneous, and with a diameter close to 50 nm (Figure 4), indicating that the particles observed in SEM are made up of smaller particles. The globular morphology reported in this work is very different from the spheres obtained by spray drying (Wang *et al*., 2008). Those spheres consist of smaller, desert rose-like particles and lack a hollow core. Self assembly may be present in this sample, as in those reported by Jaber *et al*. (2009).

The NH_4US sample SEM image also reveals some smooth surfaces and small nodular particles in the cracks, comparable to those of the previous sample. The difference is the relative amount of nodular particles to smooth surface (Figure 5a). Note that in the NH_4US sample, the nodular particles are much smaller (0.2 μm) (Figure 5d). The very small particles are not as stuck as those of NH_4CON sample and seem more faceted. In the other zones of the material, stacks of layers are observed (Figure 5a,c). Very large pores, the mouths of which are close to 4 μm in diameter, are distributed throughout (Figure 5b).

Sample NH_4US was also studied by TEM to determine whether smaller particles than those observed by SEM were present and to be sure that they were nodular (Figure 6). The particles were much more globular than expected; their diameter was <10 nm. This measure was confirmed by AFM (Figure 7). A hierarchical morphology is again proposed, *i.e*. the large globular particles observed by SEM did indeed consist of smaller spherical entities.

Sample NH_4MW had a very different morphology as it was rather homogeneous. The particles were >12 μm in diameter (Figure 8a,c). Images also reveal a scaly surface with layers that may be flat or slightly curved (Figure 8b,d).

For the sample prepared using NaOH (NaMW), no nodular particles or curved scales were found

https://doi.org/10.1346/CCMN.2010.0580305 Published online by Cambridge University Press

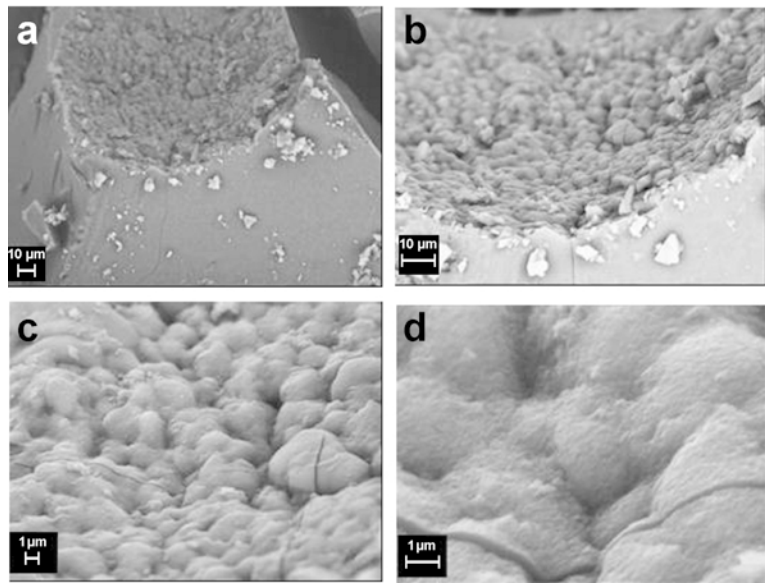


Figure 3. SEM of sample NH_4CON: (a) ×500; (b) ×1000; (c) ×2500; and (d) ×10000.

(Figure 9a). The large particles were layered (Figure 9b) and reproduced the shape already observed in equivalent preparations (Rivera *et al*., 2006).

The Kratky curves (Figure 10) obtained from the SAXS experiments do not show a peak so the morphology is, therefore, not spherical in any preparation; this contradiction is discussed below.

Texture

The BET specific surface areas of the NH_4OH samples prepared are beyond the resolution of the technique, *i.e*. close to zero and will be discussed further below. The Na-containing material has a specific surface area of 86 m^2/g, typical of the range of values reported for carbonate hydrotalcites (Benito *et al*., 2006a). The corresponding pore-size distribution was unimodal and close to 30 Å (Figure 11), a value not in agreement with the heterogeneous size distributions obtained by SAXS, the main peak of which indicates a radius of 110 Å. A broad peak with a maximum at a radius of 18 Å was also observed (Figure 11), which is in close agreement with the BJH value for a diameter of 30 Å. Note that no differences among the samples were detected by this method, whereas only the NaMW sample had a surface area and a pore-size distribution consistent with N_2 adsorption studies. The fractal dimension determined by SAXS of the NH_4CON and NH_4MW samples was 2.18 and 2.19, respectively, but 2.10 and 2.07 for NaMW and NH_4US. The features measured by each technique are compared (Table 1).

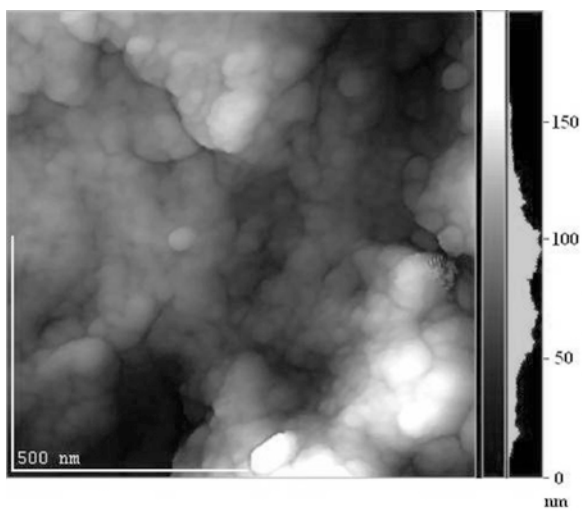


Figure 4. AFM image of sample NH_4CON. Globular particles are regular, homogeneous, and with a diameter close to 50 nm.

Thermal behavior

In a previous study (Sampieri *et al*., 2007), CO_2 retention in hydrotalcites with variable compositions was discussed and the conclusion was that the main factor affecting the retention is the metal electronegativity. As sample NH_4CON has a morphology which inhibits gas adsorption, a thermogravimetric and differential thermal analysis was performed in a CO_2 atmosphere (Figure 12). From 25 to 150ºC water was lost. From 150 to 400ºC, the weight decreased linearly from 88 to 78 wt.%. Such behavior was unexpected, as in this temperature range conventional hydrotalcites are gen-

https://doi.org/10.1346/CCMN.2010.0580305 Published online by Cambridge University Press

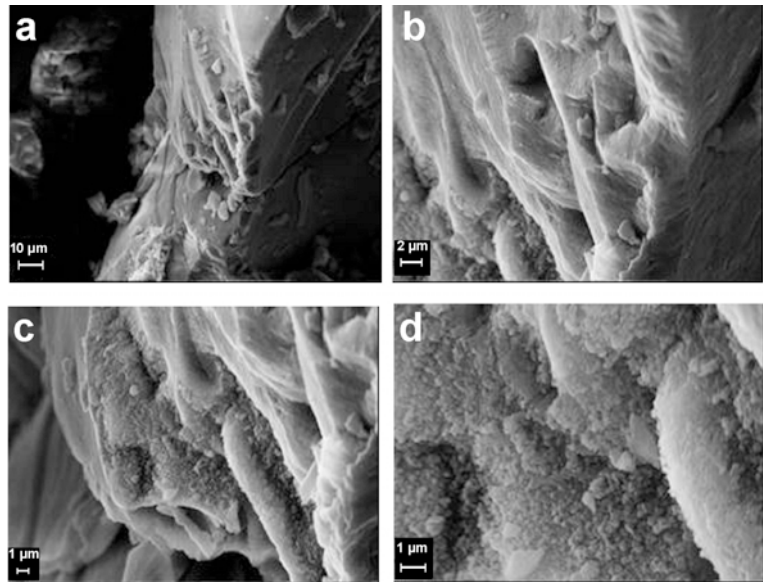


Figure 5. SEM images of sample NH_4US: (a) $\times$2500; (b) $\times$10,000; (c) $\times$10,000; and (d) $\times$25,000.

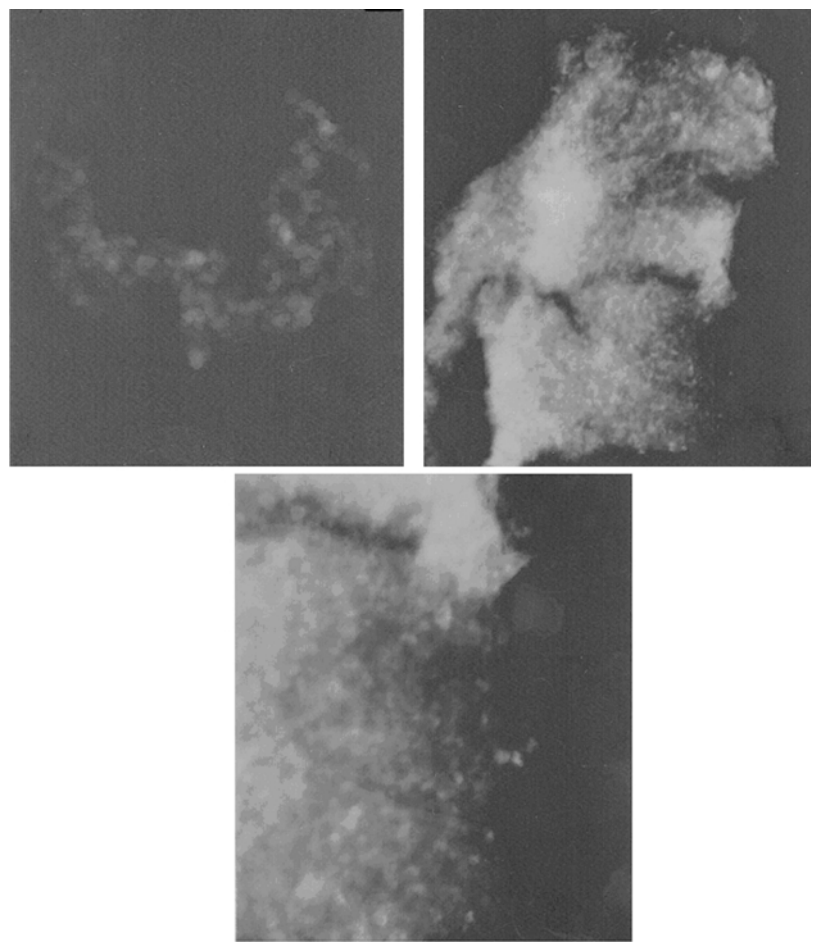


Figure 6. TEM images of sample NH_4US; particles are <10 nm across.

https://doi.org/10.1346/CCMN.2010.0580305 Published online by Cambridge University Press

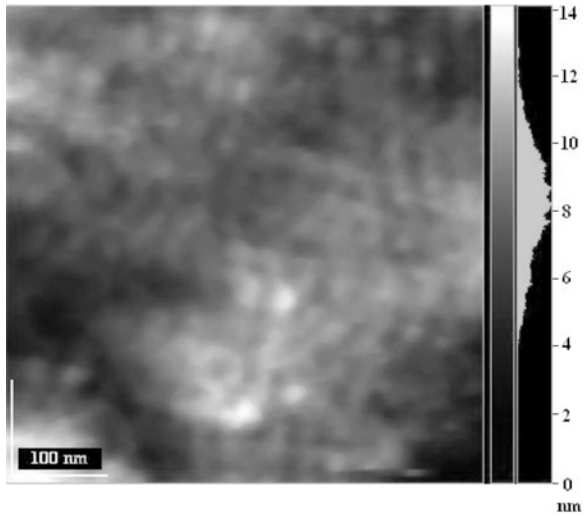


Figure 7. AFM image of sample NH_4US; particles are <10 nm across.

erally unstable (Cavani *et al*., 1991; He *et al*., 2006). Between 400 and 500ºC, the nodular agglomerates seemed to collapse as the weight decreasesd to as little as 52 wt.%. The exothermic peak in the DTA curve in the region 400–450ºC indicated that the ammonium compounds had been eliminated. Note that the decomposition of nitrate or carbonate could give rise to an endothermic peak at ~400ºC (López *et al*., 1997) in hydrotalcites prepared conventionally. The absence of this peak could be attributed to the fact that the interlayer anions (nitrates and carbonates) are still present between layers, indicating that the structure is maintained at high temperature.

The comments about thermal behavior are in agreement with the thermodiffraction patterns for the same sample (Figure 13). Corresponding diffraction patterns were obtained *in situ*, *i.e*. with the warm sample. The hydrotalcite structure was maintained in air up to 650ºC. No Mg oxides were observed, only a progressive broadening of the 003 peak, indicating more disorder in the layer stacking as stress appeared due to atomic thermal vibration.

DISCUSSION

Hydrotalcites NH_4MW and NaMW differ only in their precipitation agents, NH_4OH and NaOH, respectively. In NH_4MW, nitrates and some carbonates were intercalated, whereas in NaMW the reverse was true as shown by the interlayer distances. The samples considered (NH_4MW and NaMW) had surface areas of 0 and 86 m^2/g, respectively; this difference may be correlated to the presence, in sample NH_4MW, of N-H functional groups which avoided nitrogen permeation. Cotton and Wilkinson (1988) reported Mg complexes with NH_3 as $[Mg(NH_3)_6]^{2+}$. Such a complex could have been formed in the pore mouths of sample NH_4MW. This hypothesis is in agreement with the pore-size distributions obtained by SAXS and BJH. Gas adsorption requires open pores whereas SAXS measurements correspond to bulk analyses; the latter, therefore, include open or closed pores

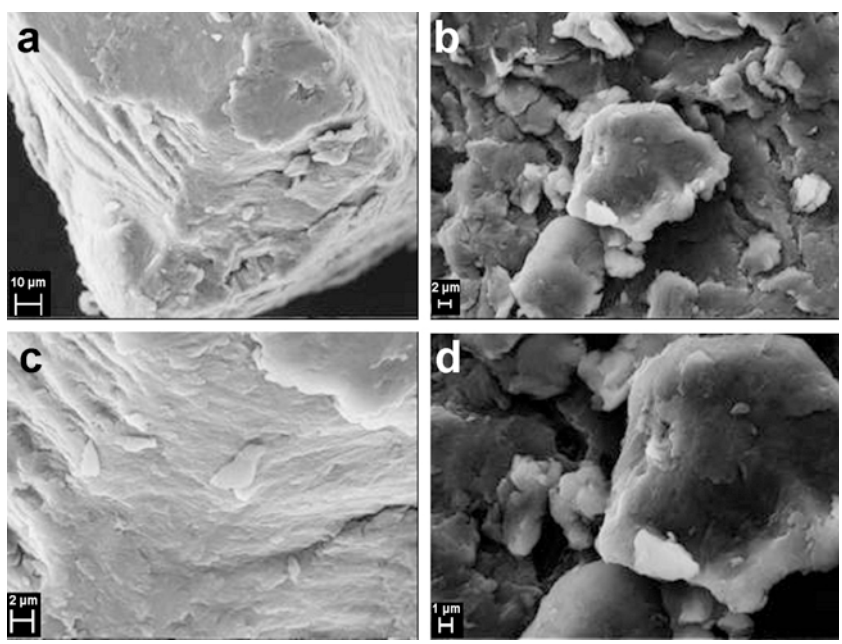


Figure 8. SEM images of sample NH_4MW: (a) ×2500; (b) ×5000; (c) ×10,000; and (d) ×10,000.

https://doi.org/10.1346/CCMN.2010.0580305 Published online by Cambridge University Press

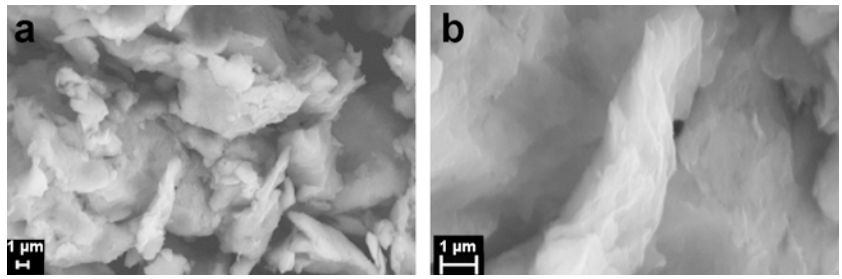


Figure 9. SEM images of sample NaMW: (a) ×2500 and (b) ×10,000.

(bubbles). Comparison of the two distributions showed that, in the NaMW sample, the open pores were 30 Å wide but that larger diameter pores determined by SAXS (220 Å diameter) were also present and not detected by the BJH method. In the NH_4MW hydrotalcite, the 30 Å pores were occluded by the proposed complex. The fractal dimension depends on the connectivity of the pore network (Harrison, 1995). In the NH_4MW it was 2.19 whereas in the NaMW it was 2.10. Such behavior may be compared with results reported for other lamellar compounds (Pernyeszi and Dékány, 2003); in montmorillonite and illite the fractal dimensions are 2.83 and 2.58, respectively, and in kaolinite it is 2.12 but in silica it is 2.01. In the present hydrotalcites, also lamellar structures, the values obtained were, therefore, in the range of other lamellar materials. NH_4MW thus contains more closed mesopores than NaMW.

If samples NH_4MW and NH_4US are compared, in order to understand the irradiation effect, the only difference is morphological. As the fractal dimensions were 2.19 and 2.07, respectively, the connectivity of sample NH_4US was less than that of NH_4MW; indeed, the NH_4US SEM images present two types of topographies, not only a lamellar one but a nodular morphology was also observed. Microwave irradiation provided high energy and promoted gas-molecule diffusion; the hydro-

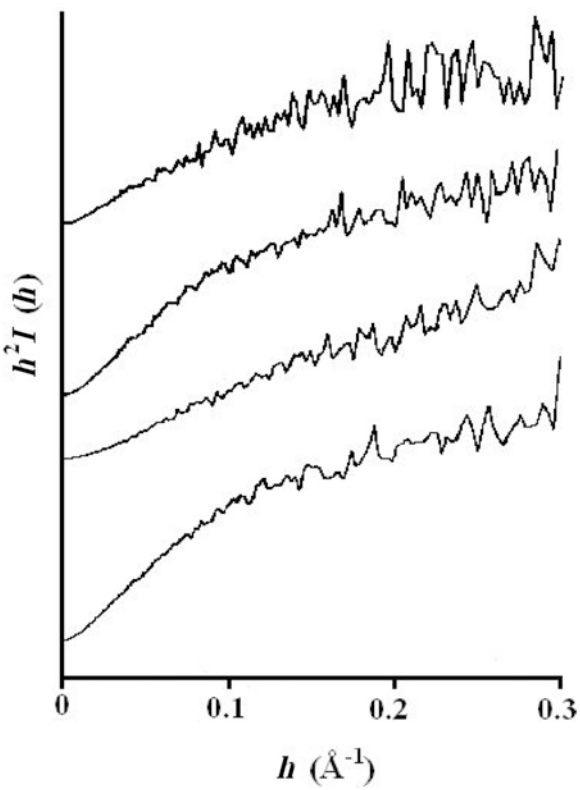


Figure 10. Kratky curves of samples: (a) NH_4US; (b) NH_4MW; (c) NaMW; and (d) NH_4CON.

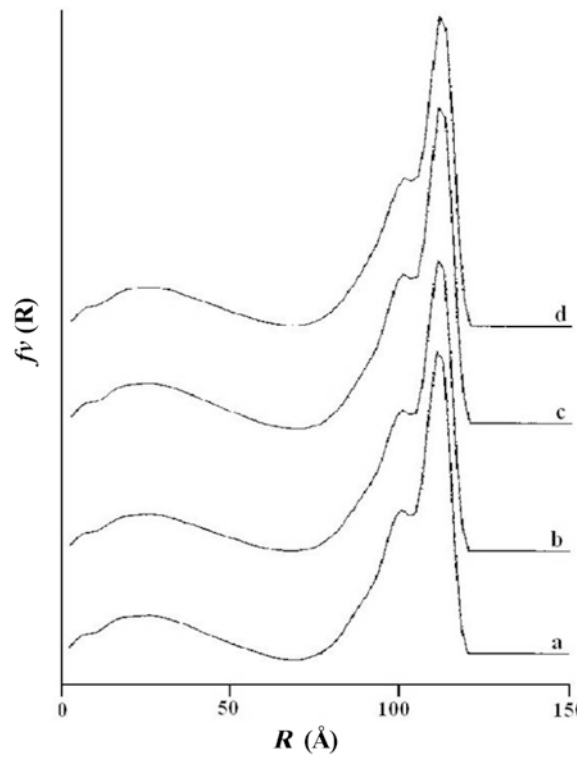


Figure 11. Size-distribution functions of samples: (a) NH_4US; (b) NH_4MW; (c) NaMW; and (d) NH_4CON.

https://doi.org/10.1346/CCMN.2010.0580305 Published online by Cambridge University Press

Table 1. Comparison of the values obtained by XRD, IR, BET, BJH, and SAXS.

Sample	Interlayer distance, by XRD (Å)	Presence of ammonium bands (IR)	Surface area (BET)	Pore-size distribution, diameter (BJH)	Pore-size distribution, radius (SAXS)	Fractal dimension (SAXS)
NH_4CON	8.4	Yes	0	–	18; 110 Å	2.18
NH_4MW	8.4	Yes	0	–	18; 110 Å	2.19
NH_4US	8.4	Yes	0	–	18; 110 Å	2.07
NaMW	7.6	No	86 m^2/g	30 Å	18; 110 Å	2.10

talcite grew rapidly and uniformly. Ultrasound irradiation is much less energetic. Each method, therefore, favors a different nucleation process (Benito *et al*., 2006b). Indeed, microwave irradiation only interacts with polar molecules, as water, whereas ultrasound irradiation excites every kind of molecule.

The present work revealed that the morphology depends mainly on the energy provided to the system due to the formation of different amounts of encapsulated gas. Microwave irradiation should promote the formation of very large gas molecule agglomerates which cannot work as templates. Ultrasound irradiation probably favors the association of few molecules; smaller amounts of gas are then released, some being small enough to serve as templates.

Such conclusions are supported by sample NH_4CON, which was synthesized conventionally in the presence of NH_4OH. A large amount of nodular particles was observed, the size of which was twenty times larger than in NH_4US. Such morphology appears to contradict the non-globular shape determined by means of the Kratky curves. In fact, SAXS operates on the basis of variations in the electron density and corresponds to heterogeneities of <300 Å. The Kratky curves and, therefore, the size-distribution curves are due to pore shapes and not to particle sizes. Those pores are more or less cylindrical. The radii determined are those of the cylinder sections (Glatter, 1988). Again, the fractal dimension varies; it is now 2.18, indicating that, as in the previous sample, pores are closed off. The micrographs show gas bubbles that explode, forming craters and cavities on the surface. Such morphology reveals the presence of gases that are liberated when the sample is a viscous gel. Two competitive nucleation processes, one ending in a lamellar morphology and the other in a nodular morphology, are proposed. In NH_4MW, the lamellar morphology is favored whereas for NH_4CON the nodular morphology predominates. Irradiation with ultrasound provides an intermediate sample. The resulting sequence was conditioned by the energy flux. Note that hydrotalcite nodules are only formed in the presence of a gas, either alcohol vapor (Valente *et al*., 2007) or NH_3.

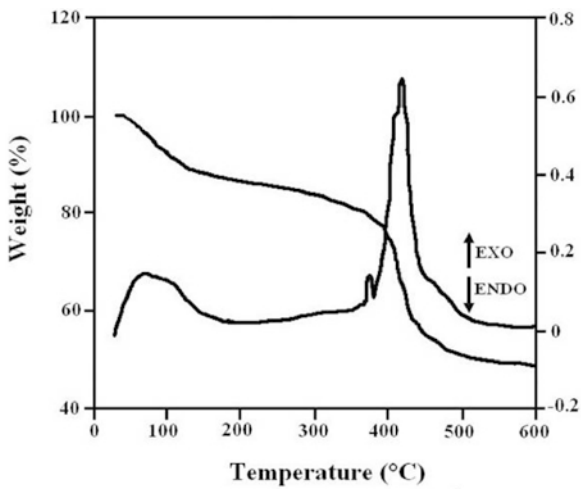


Figure 12. TGA-DTA curves of sample NH_4CON.

Water vapor, liberated during the NaOH synthesis, for sample NaMW does not work as a vesicle template because the water-vapor pressure is too high. As expected, this material has a large surface area and a layered structure. Instead, the presence of ammonium in the synthesis mixture promotes the formation of complexes such as $[Mg(NH_3)_6]^{2+}$ (Cotton and Wilkinson, 1988) which block the accessibility of surfaces to nitrogen adsorption.

The mechanism to obtain hydrotalcite nodules *via* a gaseous template is, therefore, similar to those observed in volcanic eruptions. Geodes could serve as a macroscopic model for the new materials, consisting of thick skins and small globular particles within. The proposal explains the sorption features as well as the great thermal stability of the NH_4CON sample.

CONCLUSIONS

The treatments during the hydrothermal step (conventional, microwave, or ultrasound irradiation) determine the morphology and texture of the hydrotalcite prepared in the presence of NH_4OH (precipitant) because they determine the energy flux. The effluent gas serves as the template for the nodular particles. A microscopic geode model is proposed. The materials are heterogeneous and layered morphologies are obtained

https://doi.org/10.1346/CCMN.2010.0580305 Published online by Cambridge University Press

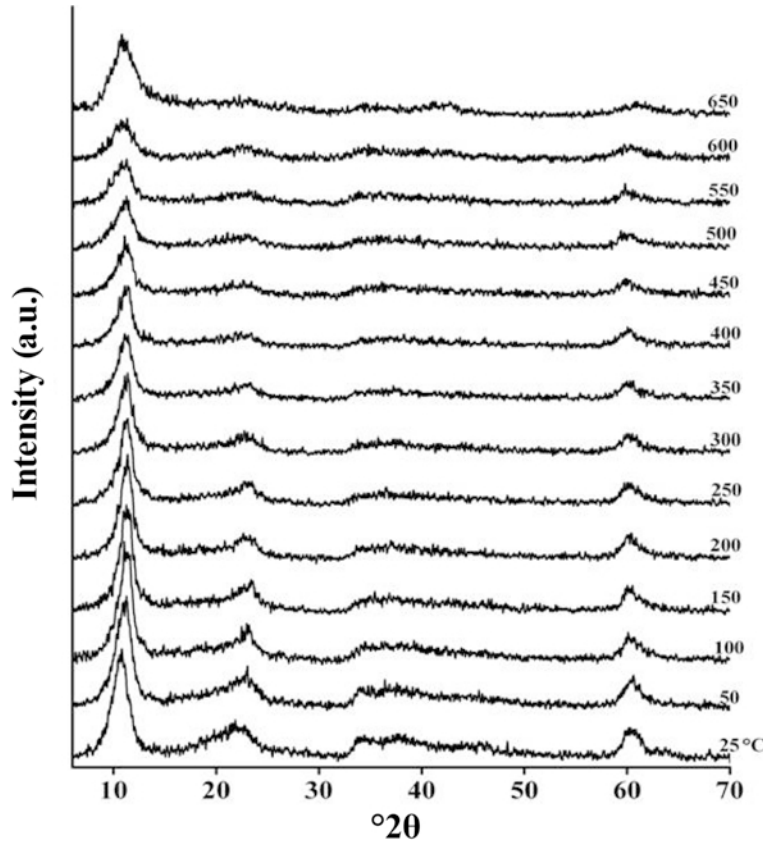


Figure 13. X-ray thermodiffraction patterns of sample NH_4CON.

simultaneously. The present results offer a new, controlled method of producing, on request, lamellar or nodular morphologies, simply by changing the precipitating agent and/or the energy flux.

Simple XRD characterization is not sufficient to understand the sorption properties of the materials prepared. The fractal dimension is useful as it can be correlated to pore connectivity, and, therefore, to pore accessibility. For this reason, SAXS analysis is recommended as it also provides the pore shape and the bulk pore-size distribution to be contrasted with the BJH analysis which corresponds to the gas-accessible surface only.

ACKNOWLEDGMENTS

The XRD, TGA-DTA, and electron microscopy work of Leticia Baños, Esteban Fregoso, and José Guzmán is gratefully acknowledged. The photography was done by E. Caballero. The study presented here would not have been possible without the UNAM-IIM library services. Financial support from CONACYT and the Nanogastor-Alfa II project is also gratefully acknowledged.

REFERENCES

Allada, R.K., Peltier, E., Navrotsky, A., Casey, W.H., Johnson, C.A., Berbeco, H.T., and Sparks, D.L. (2006) Calorimetric determination of the enthalpies of formation of hydrotalcite-like solids and their use in the geochemical modeling of metals in natural waters. *Clays and Clay Minerals*, **54**, 409–417.

Benito, P., Labajos, F.M., and Rives, V. (2006a) Uniform fast growth of hydrotalcite-like compounds. *Crystal Growth Design*, **6**, 1961–1966.

Benito, P., Labajos, F.M., Rocha, J., and Rives, V. (2006b) Influence of microwave radiation on the textural properties of layered double hydroxides. *Microporous and Mesoporous Materials*, **94**, 148–158.

Cavani, F., Trifiro, F., and Vaccari, A. (1991) Hydrotalcite-type anionic clays: preparation, properties and applications. *Catalysis Today*, **11**, 173–301.

Cotton, F.A. and Wilkinson, G. (1988) *Química Inorgánica Avanzada*. Limusa, Mexico.

Evans, D.G. and Slade, R.C.T. (2006) Structural aspects of layered double hydroxides. *Structure and Bonding*, **119**, 1–87.

Glatter, O. and Gruber, K. (1993) Indirect transformation in reciprocal space: desmearing of small-angle scattering data from partially ordered systems. *Journal of Applied Crystallography*, **26**, 512–518.

Glatter, O. (1998) Comparison of two different methods for direct structure analysis from small-angle scattering data. *Journal of Applied Crystallography*, **21**, 886–890.

Harrison, A. (editor) (1995) *Fractals in Chemistry.* Oxford University Press Inc., New York.

He, J., Wei, M., Li, B., Kang, Y., Evans, D.G., and Duan, X. (2006) Preparation of layered double hydroxides. *Structure and Bonding*, **119**, 89–119.

Hernandez-Moreno, M.J., Ulibarri, M.A., Rendon, J.L., and

https://doi.org/10.1346/CCMN.2010.0580305 Published online by Cambridge University Press

Serna, C.J. (1985) IR characteristics of hydrotalcite-like compounds. *Physics and Chemistry of Minerals*, **12**, 34–38.

Jaber, M., Gaslain, F.O.M., and Miehé-Brendlé, J. (2009) Rapid and direct synthesis of spherical organoclay. *Clays and Clay Minerals*, **57**, 35–39.

Kim, M.-H. (2004) Modified Porods law estimated of the transition-layer thickness between two phases: test of triangular smooting function. *Journal of Applied Crystallography*, **37**, 643–651.

Lei, X., Yang, L., Zhang, F., and Duan, X. (2006) A novel gas-liquid contacting route for the synthesis of layered double hydroxides by decomposition of ammonium carbonate. *Chemical Engineering Science*, **61**, 2730–2735.

Li, F. and Duan, X. (2006) Applications of layered double hydroxides. *Structure and Bonding*, **119**, 193–223.

Lopez, T., Bosch, P., Ramos, E., Gomez, R., Novaro, O., Acosta, D., and Figueras, F. (1996) Synthesis and characterization of sol-gel hydrotalcites. Structure and texture. *Langmuir*, **12**, 189–192.

Lopez, T., Bosch, P., Asomoza, M., Gómez, R., and Ramos, E. (1997) DTA-TGA and FTIR spectroscopies of sol-gel hydrotalcites: aluminium source effect on physicochemical properties. *Materials Letters*, **31**, 311–316.

Martin, J.E. and Hurd, A.J. (1987) Scattering from fractals. *Journal of Applied Crystallography*, **20**, 61–78.

Méheust, Y., Dagois-Bohy, S., Knudsen, K.D., and Fossum, J.O. (2007) Mesoscopic structure of dry-pressed clay samples from small-angle X-ray scattering measurements. *Journal of Applied Crystallography*, **40**, s286–s291.

Olanrewaju, J., Newalkar, B.L., Mancino, C., and Komarneni, S. (2000) Simplified synthesis of nitrate form of layered double hydroxide. *Materials Letters*, **45**, 307–310.

Paredes, S.P., Fetter, G., Bosch, P., and Bulbulian, S. (2006) Sol-gel synthesis of hydrotalcite-like compounds. *Journal of Materials Science*, **41**, 3377–3382.

Pernyeszi, T. and Dékány, I. (2003) Surface fractal and structural properties of layered clay minerals monitored by small-angle X-ray scattering and low-temperature nitrogen adsorption experiments. *Colloid and Polymer Science*, **281**, 73–78.

Pretsch, E., Bühlmann, P., and Affolter, C. (2000) *Structure Determination of Organic Compounds*. Springer, Zürich.

Rivera, J.A., Fetter, G., and Bosch, P. (2006) Microwave power effect on hydrotalcite synthesis. *Microporous and Mesoporous Materials*, **89**, 306–314.

Rivera, J.A., Fetter, G., Giménez, Y., Xochipa, M.M., and Bosch, P. (2007) Nickel distribution in (Ni,Mg)/Al-layered double hydroxides. *Applied Catalysis A*, **316**, 207–211.

Rives, V. and Ulibarri, M.A. (1999) Layered double hydroxides (LDH) intercalated with metal coordination compounds and oxometalates. *Coordination Chemistry Reviews*, **181**, 61–120.

Sampieri, A., Fetter, G., Pfeiffer, H., and Bosch, P. (2007) Carbonate phobic (Zn,Mn)-Al hydrotalcite-like compounds. *Solid State Sciences*, **9**, 394–403.

Sels, B.F., de Vos, D.E., and Jacobs, P.A. (2001) Hydrotalcite-like anionic clays in catalytic organic reactions. *Catalysis Reviews*, **43**, 443–488.

Tichit, D. and Vaccari, A. (1998) Recent catalytic applications of hydrotalcite-type anionic clays. *Applied Clay Science*, **13**, 311–326.

Valente, J.S., Cantú, M.S., Cortez, J.G.H., Montiel, R., Bokhimi, X., and López-Salinas, E. (2007) Preparation and characterization of sol-gel MgAl hydrotalcites with nanocapsular morphology. *Journal of Physical Chemistry C*, **111**, 642–651.

Wang, Y., Zhang, F., Xu, S., Wang, X., Evans, D.G., and Duan, X. (2008) Preparation of layered double hydroxide microspheres by spray drying. *Industrial Engineering Chemistry Research*, **47**, 5746–5750.

(*Received 23 March 2009; revised 3 December 2009; Ms. 297; A.E. F. Bergaya*)

https://doi.org/10.1346/CCMN.2010.0580305 Published online by Cambridge University Press